Journal of Inorganic and Organometallic Polymers and Materials
https://doi.org/10.1007/s10904-019-01280-3

Photocatalytic Degradation of 2,4-Dichlorophenoxyacetic Acid in Aqueous Solution Using Mn-doped ZnO/Graphene Nanocomposite Under LED Radiation

Roya Ebrahimi[1] · Mahnaz Mohammadi[1] · Afshin Maleki[1] · Ali Jafari[2] · Behzad Shahmoradi[1] · Reza Rezaee[1] · Mahdi Safari[1] · Hiua Daraei[1] · Omid Giahi[1] · Kaan Yetilmezsoy[3] · Shivaraju Harikaranahalli Puttaiah[4]

Received: 21 April 2019 / Accepted: 3 August 2019

Abstract

Chemical pesticides and herbicides are one of the most important pollutants in urban, agricultural and industrial wastewaters. Improper discharge of these compounds into water bodies' cause harmful effects on both environment and human health. In this study, photocatalytic degradation of 2,4-Dichlorophenoxyacetic acid (usually called 2,4-D) was investigated using Mn-doped zinc oxide/graphene nanocomposite under light emitting diodes (LED) radiation. FTIR, AFM, DLS, Zeta potential, XRD, and SEM techniques were used to determine the characteristics of the nanocomposite. The effects of process-related parameters, such as the amount of nanocomposite, initial pH, 2,4-D concentrations, and contact time, on the photocatalytic degradation of the 2,4-D were studied. The results showed that the efficiency of photocatalytic degradation of 2,4-D decreased with an increase in the initial concentration of 2,4-D, while photocatalytic degradation efficiency increased by increasing the initial pH and the nano-catalyst content. The results showed that 66.2% of 2,4-D could be photocatalytically degraded using Mn-doped zinc oxide/graphene nanocomposite under LED radiation at optimal conditions (pH 5, initial Zn concentration of 10 mg L^{-1}, nano-composite concentration of 2 g L^{-1}, contact time of 120 min). Findings of this experimental study concluded that photocatalysis using Mn-doped zinc oxide/graphene nanocomposite under LED radiation could efficiently remove 2,4-D herbicide from aqueous media.

Keywords LED radiation · ZnO · Nanocomposite · 2,4-Dichlorophenoxyacetic acid · Graphene

✉ Afshin Maleki
maleki43@yahoo.com; malaki@muk.ac.ir

✉ Kaan Yetilmezsoy
yetilmez@yildiz.edu.tr; kyetilmezsoy@gmail.com

Roya Ebrahimi
ebrahimi83@yahoo.com

Mahnaz Mohammadi
m.mohammadi7@yahoo.com

Ali Jafari
jafari_a99@yahoo.com

Behzad Shahmoradi
bshahmorady@gmail.com

Reza Rezaee
rezaee.eng@gmail.com

Mahdi Safari
safari.m.eng@gmail.com

Hiua Daraei
hiua.daraei@gmail.com

Omid Giahi
omidgi71@yahoo.com

Shivaraju Harikaranahalli Puttaiah
shivarajuenvi@gmail.com

1 Environmental Health Research Center, Research Institute for Health Development, Kurdistan University of Medical Sciences, Sanandaj, Iran

2 School of Health, Lorestan University of Medical Sciences, Khorramabad, Iran

3 Department of Environmental Engineering, Faculty of Civil Engineering, Yildiz Technical University, Davutpasa Campus, Esenler, 34220 Istanbul, Turkey

4 Department of Water and Health, Faculty of Life Sciences, Jagadguru Sri Shivarathreeshwara University, Sri Shivarathreeshwara Nagara, Mysuru, Karnataka 570015, India

Published online: 10 August 2019

1 Introduction

Chlorinated phenoxyacetic acid compounds are important groups of herbicides that are widely utilized in the agriculture for controlling the growth of weeds [1, 2]. Among these compounds, 2,4-Dichlorophenoxyacetic acid (2,4-D) has been widely used due to its high solubility, toxicity and long-term stability in the environment [3]. The US Environmental Protection Agency (US EPA) classified 2,4-D as a priority pollutant [4]. For 2,4-D, World Health Organization (WHO) set the discharge standard as 1 mg L^{-1} [5]. Acute adverse effects of this contaminant include irritation of eyes, skin and throat, and respiratory problems. Moreover, its long-term effects cover central nervous system weakness, muscle weakness, and liver and kidney problems [6].

Different physical, chemical, and biological methods including chemical oxidation, membrane process, electrochemical process, ion exchange, adsorption and photocatalytic methods have been investigated for the removal of 2,4-D from aqueous solutions [7–9]. Among them, photocatalytic degradation has been emphasized as one of the most effective methods for elimination of these pollutants. In conventional photocatalytic techniques, a UV light source (e.g. a low-pressure mercury vapor lamp) and a semiconductor catalyst are used [10]. However, these lamps are regarded to be an environmental hazard and uneconomical due to high toxicity of mercury, relatively short effective life, and high energy intensity [11]. Nowadays, light emitting diodes (LED) lamps are known as a suitable alternative for mercury lamps in photocatalytic degradation processes because of their less toxicity, long life, high energy efficiency, direct electrical conductivity, and high flexibility in optical reactors [12].

In the most of photocatalytic processes, nanoparticles, such as titanium dioxide [13, 14] and zinc oxide, [15] are used as catalyst. For instance, zinc oxide has been used to degrade various organic compounds due to the its direct gap band energy, the binding energy of 60 MeV (mega-electronvolt), resistance to light and chemical corrosion, no toxicity, insolubility, capability of wide range of electromagnetic waves absorption, and excellent photocatalytic properties as a semi-conductor catalyst [16, 17]. Graphene is a graphite layer and is a 2-D carbon allotropic with a grid-like structure such as a honeycomb. It is used as building blocks of carbon nanotubes and large fullerenes [18]. At the nano size, graphene has significant properties such as its high Young modulus (about 1000 GPa: gigapascal), high resistance to failure (130 GPa), good thermal conductivity (5000 W m^{-1} K^{-1}), electrical conductivity (200000 cm^2 V^{-1} s^{-1}), specific surface area (2600 m^2 g^{-1}), owning catalytic properties, and amazing transport phenomena (e.g. the quantum Hall effect, adsorption of some metal ions and pollutants from soil and water) [15, 16]. On the other hand, doping of semiconductors with metals is one way to increase the photocatalytic activity of them. Indeed, it causes alteration of the energy gap and increasing light adsorption, thereby zinc oxide exhibits its photocatalytic activity in the visible light region. Recently, doping with Mn has been considered because of its high efficiency in changing the energy gap. It is noted that the amount of Mn in this process is very important, and the doping efficiency is directly related to the concentration of Mn used. ZnO can also be placed on a surface, such as zeolite, alumina, silica, and graphene, to increase the doping efficiency due to comfort motion of its electron [18–20]. Based on the foregoing facts, the purpose of the present study was to synthesize Mn-doped ZnO/graphene nanocomposite and to determine of its ability in degradation of 2,4-D under LED radiation.

2 Materials and Methods

2.1 Chemicals

2,4-D was purchased from Meshkfam Chemical Company (Iran). Other chemicals, such as graphene oxide (GO), manganese acetate, zinc acetate, sulfuric acid, and nitric acid, were laboratory grade and obtained from Merck (Germany). The chemical structure, chemical and physical properties of 2,4-D are shown in Table 1.

2.2 Preparation of Mn-doped ZnO/GO

Solvothermal method was used to prepare Mn-doped ZnO/GO nanocomposite. In the first step, GO (10% of by weight) was dissolved in 80 mL ethylene glycol (EG) under ultrasound for 2 h at ambient temperature. Then, manganese acetate (5% by weight) and 80 mg zinc acetate were dissolved in 80 mL EG and added into the GO solution under stirring conditions. After that, 20 mL of NaOH (0.1 N) were added to the above mixture and stirred for 1 h to obtain a homogenous suspension. The suspension was then transferred to a stainless-steel autoclave and stored at 160 °C for 24 h. Finally, the prepared composite was obtained by centrifugation and five times washing with pure ethanol and distilled water. Finally, the product was dried in a vacuum oven at 80 °C for 24 h [19].

2.3 Experimental Methodology

In this study, photocatalytic degradation of 2,4-D herbicide was investigated by using a synthesized nanocomposite in a 100-mL batch reactor. At first, a stock solution of 2,4-D

Table 1 Structure and characteristics of 2,4-Dichlorophenoxyacetic acid

Chemical formula	$C_8H_6Cl_2O_3$
Skeletal formula	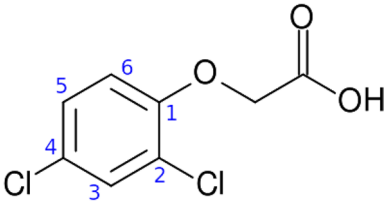
3D representation	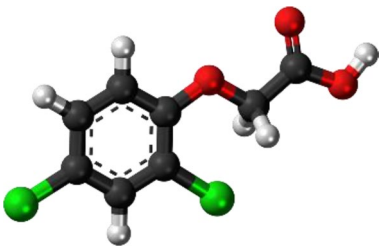
Class	Herbicide
Group	Phenoxy carboxylic acid
Hazard group	Weak toxicity (III)
Molecular weight	221.04 g mol^{-1}
Boiling point	160 °C (320 °F; 433 K) 0.4 mm Hg
Melting point	140.5 °C (284.9 °F; 413.6 K)
Solubility in water	900 mg L^{-1}
Toxicity grade	700–160 mg L^{-1}
Appearance	White to yellow powder
CAS (chemical abstracts service) number	94-75-7
European community (EC) number	202-361-1

(1000 mg L^{-1}) was prepared. Then, different concentrations of the herbicide were prepared from the stock solution and transferred to the batch reactor. Different amounts of the synthesized nanocomposite were added to the reactor, and LED lamps were turned on. After a pre-defined time, the concentration of 2,4-D in the reactor was measured. At each step, the efficiency of removal and the effect of the existing parameters were investigated by changing only one parameter and keeping other parameters constant. In this study, the operating parameters, such as amount of nanocomposite (0.5, 1, 2, and 3 g L^{-1}), initial concentrations of 2,4-D (10, 25, 50, 75, and 100 mg L^{-1}), initial pH (3, 5, 7, 9, and 11), and the reaction time (20 to 120 min) were investigated.

2.4 Analytical Methods

The concentrations of 2,4-D were measured by a spectrophotometer (DR5000-HACH) at 280 nm wavelength before and after the reaction [20]. Scanning Electron Microscopy (SEM) (TESCAN, Czech Republic) was used to explore the morphology of the synthesized nanoparticles. Structural properties of nanoparticles were also analyzed using X-Ray Diffraction (XRD) methodology (Model: X'Pert PRO MPD, the Netherlands). Furthermore, functional groups on the surface of the nanoparticles were determined by using the Infrared Fourier Transform Spectrometer (FTIR) (Bruker, Model: Tensor 27, Germany). A particle sizer (DLS: Dynamic Light Scattering) and zeta potential analyzer (Nanobrook Omni, Brookhaven Instruments Corporation, USA) were used to measure the electric potential at the surface of the nanoparticles and nanoparticle size distributions. Moreover, the surface topography and roughness of the Mn-doped ZnO/GO were analyzed by using atomic force microscope (AFM) (Ara-Research, Model: Advance, Iran).

3 Results and Discussion

3.1 Nanophotocatalyst Characteristics

Figure 1 illustrates the SEM images of GO sheet and Mn-doped ZnO/GO nanocomposite. As seen from Fig. 1a, the GO structure is transparent, and single-layered and low-layer sheets are existed. Also, the side fracture of the GO sheets confirmed the layered structure of all parts of GO. The addition of ZnO nanoparticles and Mn to GO created a granular

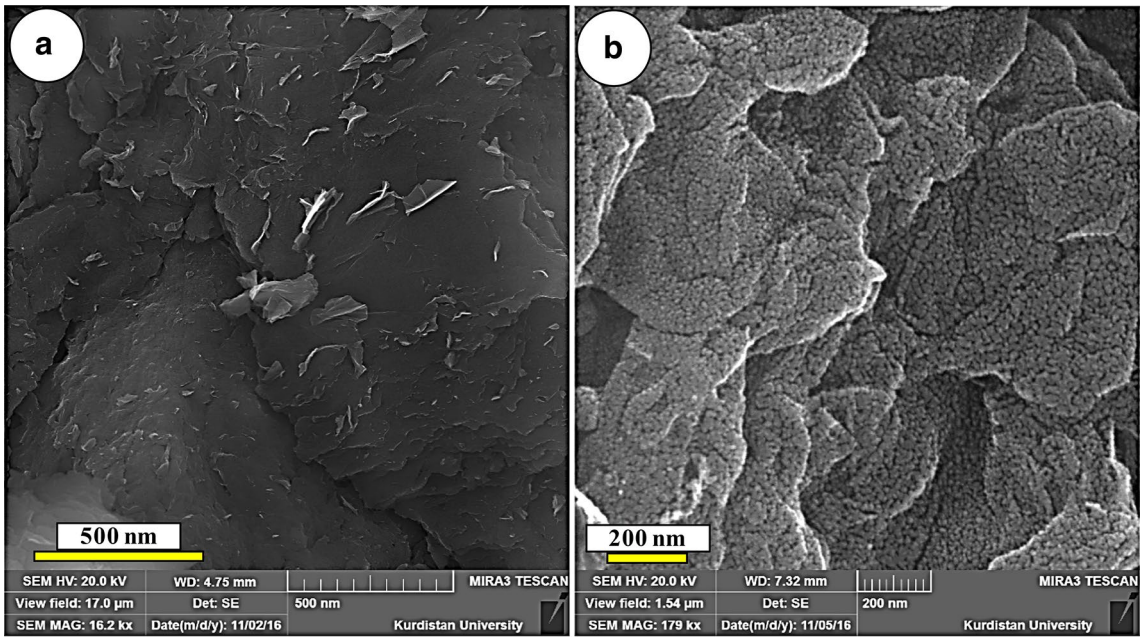

Fig. 1 SEM image of **a** GO and **b** Mn doped ZnO/GO nanocomposite

appearance (Fig. 1b). The spherical and dense particles (with a mean size of 20 to 40 nm) are normally distributed onto graphene layers. This size is in accordance with the particle size obtained from the Scherrer's equation via the XRD analysis.

Figure 2a shows the FTIR spectra of the Mn-doped ZnO/GO nanocomposite. As seen from in Fig. 2a, the results obtained from FTIR shows that the peaks appearing at 3458, 2923, and 1051 cm^{-1} are assigned to stretching vibrations of OH, CH, and the C–O functional groups, respectively. Another peak appearing in 1627 cm^{-1} corresponds to the stretching vibration of the C=C bond. The peaks appeared at 532, 543, and 450 cm^{-1} are assigned to the presence of metal groups in composition. Since in sol–thermal process GO is first reduced and then the nanocomposite is synthesized, the peak appearing at 3467 cm^{-1} is related to the presence of zinc groups on the graphene structure. The peak observed at 439 cm^{-1} also indicates the presence of Mn in the composition [21, 22].

XRD analysis was used to characterize the crystalline nature and phase purity of GO, ZnO/GO, and Mn-doped ZnO/GO nanoparticles. Figure 2b–d illustrate the X-ray diffraction patterns of all prepared samples recorded in the range of 20° to 120°. As seen from Fig. 2b, the characteristic peak at $2\theta = 11°$ was assigned to the (001) plane of GO and indicated the effective oxidation of graphite and also the formation of GO [19, 23, 24]. In the XRD pattern of GO, the (001) crystal plane of GO was evident, which was typical for GO [25]. This result was in a good agreement with other published reports who stated that the XRD peak should shift from ~ 26° to ~ 11° when the graphite was oxidized and became GO [24, 26]. However, after the reduction of GO to graphene, the diffraction peak at 11° disappeared, and two small peaks at ~ 25° and ~ 43° were observed, which could be ascribed to graphene (002) and (100) planes [19, 27]. Hence, GO was reduced to graphene by the solvothermal process. The characteristic peak located at $2\theta = 31°$, 34°, 37°, 48°, 56°, 61°, and 68° were attributed to lattice planes (100), (002), (101), (102), (110), (103), and (112), respectively. This revealed that the synthesized nanoparticles exhibited a good crystalline nature with wurtzite hexagonal structure (JCPDS card 01-075-1533) [19, 28]. The XRD pattern of Mn-ZnO/GO confirmed that there was no additional peak for Mn-related secondary phase (Fig. 2c). However, a small hump was observed at $2\theta = 25°$ in the XRD pattern of ZnO/GO (Fig. 2c) and Mn-doped ZnO/GO (Fig. 2d), which were related to the (002) plane of graphene and demonstrated the conversion of GO into reduced GO [29, 30]. This result showed that the Mn-doped ZnO/GO nanoparticles were well-decorated on the graphene sheets [19].

According to the Scherrer's equation (Eq. 1), the size of the GO/ZnO nanoparticles is about 35.2 nm, and the size of the Mn-doped ZnO/GO nanocomposite is 35 nm. This showed that addition of Mn decreased the particle size. This difference may be due to the magnetic property of Mn. The magnetic interaction between Zn and Mn ions was more than the magnetic interaction between Zn ions. As a result, the length of the ion bonds of Zn–Mn was less than that of Zn–Zn, resulting in a decrease in size of the nanoparticles. In addition, the results showed that,

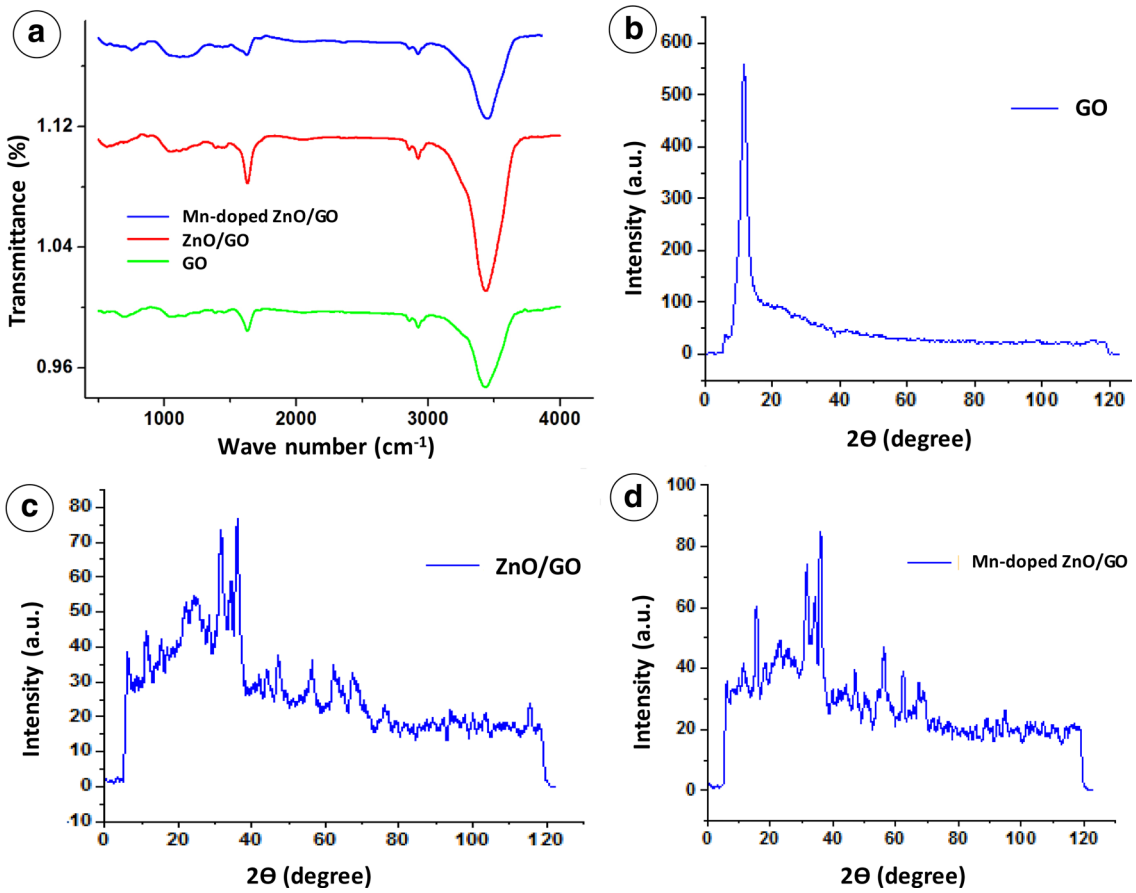

Fig. 2 **a** FTIR spectra of prepared nanocomposites; **b** XRD pattern of GO; **c** XRD pattern of ZnO/GO; and **d** XRD pattern of Mn doped ZnO/GO nanocomposite

Table 2 Network parameters of nanocomposite

Nanocomposite	Nanoparticles size (nm)	a (Å)	c (Å)	c/a ratio	Volume (Å^3)
ZnO/GO	35.2	3.249	5.2070	1.6026	27.4825
Mn doped ZnO/GO	35	5.84	5.84	1	99.5883

the network constants increased with the addition of Mn due to replacement of Mn^{2+} ion (with radius of 0.62 Å) instead of Zn^{2+} (with an ionic radius of 6.0 Å) [31]. The parameters for the nanocomposite network are presented in Table 2. The Scherrer's equation is expressed as follows:

$$D = \frac{K\lambda}{\beta \cos\theta} \quad (1)$$

where D is the crystal size in nm, β is the width of the peak at half of maximum intensity in radians, θ is the peak angle of the Bragg angle in terms of degrees, and λ of the X-ray wavelength in nm.

The two- and three-dimensional AFM images of graphene/ZnO in contact mode (with a scanning distance of 3 × 3 μm) is shown in Fig. 3. The results of the analysis of the sizes and roughness coefficients of the nanoparticles are also illustrated in Fig. 3. According to AFM analysis, the diameter of the nanoparticles was 37 nm (which is consistent with XRD results), and the size between GO layers is 3–5 nm. Figure 3a also shows the alone GO layers. In this image, the red arrows demonstrate that the three distinct GO layers are well detectable. In fact, its shape indicates a few-layered sheet with a mean thickness of 1.48 nm. Figure 3b clearly shows the GO layers and coated nanoparticles (green arrows demonstrate the position of nanoparticles on a GO layer based on a two-dimensional AFM image). The deposition of nanoparticles on graphene oxide is well-seen in the three-dimensional AMF image (Fig. 3c).

One of the most important parameters for describing the colloidal dispersion stability is the zeta potential. This measurement is related to the determination of the negative charge around the double layer related to the colloidal particle due to the ionization of different functional groups. It has been found that if the zeta potential

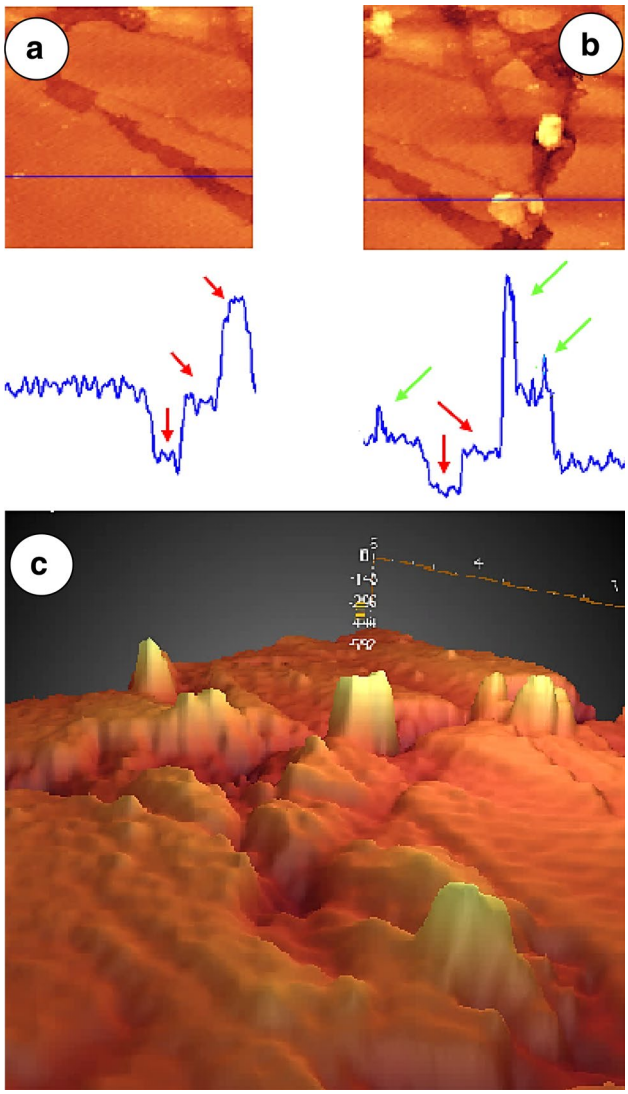

Fig. 3 AFM images of **a** GO and **b**, **c** Mn doped ZnO/GO nanocomposite

is between − 30 and + 30 mV, the particles are stable due to the distribution [32]. The surface charge may depend on the amount and type of functional groups on the surface of the GO. During the synthesis of GO, functional groups (e.g. epoxy, hydroxyl, and carboxylic groups) are located on the GO sheets. The hydroxyl and carboxylic groups of the GO sheets can weakly develop negative charges in the solution [33]. Therefore, the negative charges of the GO and Mn-doped ZnO/GO were evaluated by zeta potential measurements at the natural pH of the dispersions at 25 °C. The results are presented in Table 3; Fig. 4a, b. As seen from Table 3, the surface charge of the GO and Mn-doped ZnO/GO is − 4.75 mV and − 6.02 mV, respectively, with an increase in the surface charge of the GO after the modification. This may be due to a reduction in the agglomeration of the sheets and the presence of more carboxylic groups on the surface, and finally increase of colloidal stability.

Figure 4c, d shows the dynamic light scattering (DLS) results of GO sheet and Mn- doped ZnO/GO with a slight difference between them. For the GO sample, the size distribution varied in the range of 55 to 1100 nm with an average size of 210 nm (Fig. 4c). This means that these dispersions had a very broad size distribution and may contain large particles or agglomerates and maybe not suitable for determining size with DLS. However, these sizes were reduced after the modification of GO and reached about 160 nm (average size) at a range of 20 to 900 nm (Fig. 4d). This can be related to a reduction in the agglomeration of the sheets. In general, it is important to note that the DLS analysis assumes that particles are spherical shape. For GO, which possess extremely large ratios of length or breadth to a few nanometers thickness, these results seem logical and help to determine and to compare the relative change in the platelet size as a function of surface modification.

3.2 Effects of Operational Parameters

3.2.1 Effect of pH

The effect of initial pH on the photocatalytic degradation efficiency of 2,4-D using the Mn-doped ZnO/GO nanocomposite under the LED lamp is shown in Fig. 5a. This study was carried out at various pH values (3, 5, 7, 9, and 11), 2,4-D concentration of 50 mg L^{-1}, and Mn-doped ZnO/GO nanocomposite of 1 g L^{-1}. Based on the results, it was found that increasing the initial pH from 3 to 5 increased the removal efficiency, while a further increase of pH from 5 to 11 decreased the 2,4-D removal efficiency. The highest removal (46.5%) in photocatalytic decomposition of 2,4-D was obtained at pH value of 5.

In general, the effect of pH on the photocatalytic degradation depends on the type of pollutant and photocatalyst zero point of charge (zpc) [34]. In this study, the pH at zero point of charge (pH_{zpc}) for Mn-doped ZnO/GO nanocomposite was 7.3. According to previous studies, pK_a ($pK_a = -\log_{10}K_a$, where K_a is the negative 10-base logarithm of the acid dissociation constant) for 2,4-D was 2.8 [35] at a pH greater than this value. 2,4-D charge was negative while Mn doped ZnO/GO nanocomposite charge at pH values less than 7.3 was positive. Therefore, when pH is between pK_a and pH_{zpc}, the positively charged nanocomposite adsorbs negatively charged 2,4-D, thereby increasing the photocatalytic degradation efficiency of 2,4-D.

At higher and lower pH values, repulsion forces between 2,4-D and nano-composite result in a decrease in the photocatalytic degradation of 2,4-D due to the negative charges. The results of the present study are consistent with the findings of Azari et al. [36], which showed the highest removal

Table 3 Zeta potential (PALS method) details of GO and Mn doped ZnO/GO nanocomposite

Sample	Nanomaterial	Type	Zeta potential (mV)	Mobility (μ/s)/(V/cm)	Conductance (μS)	RMS residual
1	GO	PALS	−18.65	−1.46	40	2.0933E−02
2	GO	PALS	−21.10	−1.65	40	1.7245E−02
3	GO	PALS	−18.12	−1.42	40	1.9758E−02
	Mean		−19.29	−1.51	40	1.9312E−02
	Std Err		0.92	0.07	0	1.0877E−03
	Std Dev		1.59	0.12	0	1.8839E−03
1	Mn doped ZnO/GO	PALS	−11.30	−0.88	46	1.5728E−02
2	Mn doped ZnO/GO	PALS	−11.51	−0.90	46	1.5202E−02
3	Mn doped ZnO/GO	PALS	−13.25	−1.04	46	1.8897E−02
	Mean		−12.02	−0.94	46	1.6609E−02
	Std Err		0.62	0.05	0	1.1543E−03
	Std Dev		1.07	0.08	0	1.9992E−03

GO graphene oxide, *PALS* phase analysis light scattering, *RMS* root mean square, *Std Err* standard error, *Std Dev* standard deviation

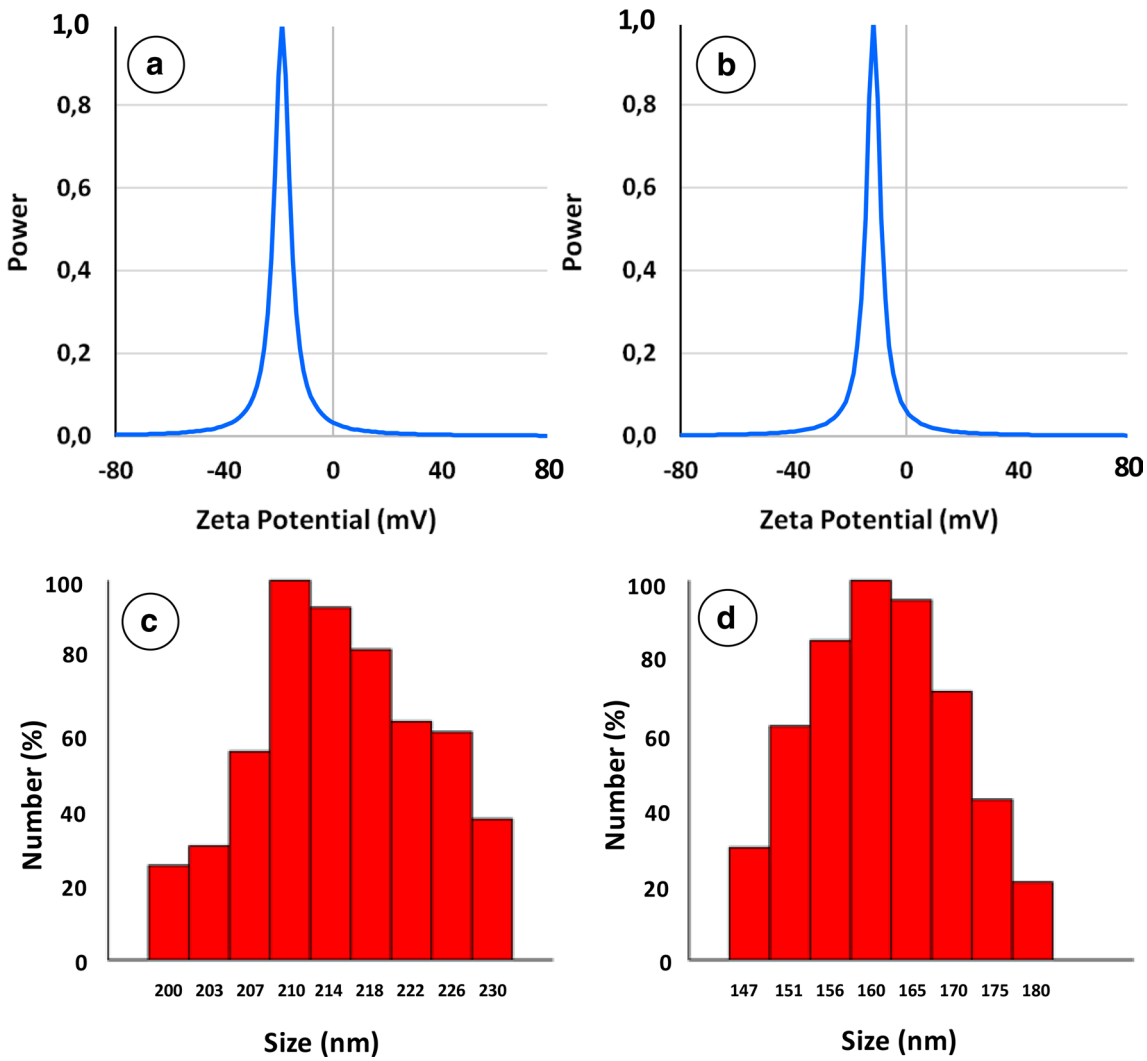

Fig. 4 Zeta potential (ELS method) of **a** GO and **b** Mn doped ZnO/GO nanocomposite; DLS of **c** GO and **d** Mn doped ZnO/GO nanocomposite

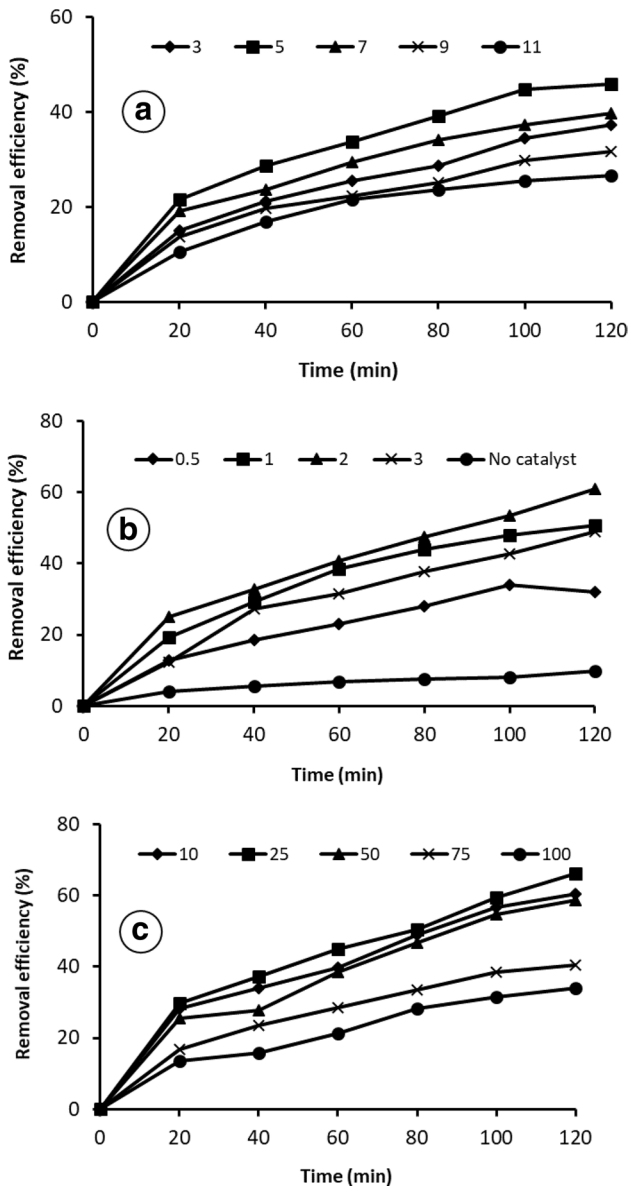

Fig. 5 **a** Initial pH effect on the photocatalytic degradation of 2,4-D under LED radiation (nanocomposite amount = 1 g/L, 2,4-D concentration = 50 mg/L); **b** effect of nanocomposite amount (g/L) on the photocatalytic degradation of 2,4-D (pH 5; 2,4-D concentration = 50 mg/L); and **c** Effect of initial concentration of 2,4-D (mg/L) on the photocatalytic degradation of 2,4-D (nanocomposite amount = 2 g/L, pH 5)

efficiency of 2,4-D at pH 5, as well as the results obtained from the study by Piri et al. [37], which obtained 89.3% removal of 2,4-D at pH value of 5.

3.2.2 Effect of Nanocomposite Amount

The effect of nanocomposite amount on photocatalytic degradation of 2,4-D under LED radiation at nanocomposite doses (0.5, 1, 2, and g L^{-1}), 2,4-D concentration of 50 mg L^{-1}, and pH 5 is given in Fig. 5b. The results showed that the photocatalytic degradation efficiency of 2,4-D in absence of Mn doped ZnO/GO nanocomposite is low and negligible, while the degradation efficiency increased with an increase in the nanocatalyst doses from 0.5 to 3 g L^{-1}. The highest removal efficiency of 2,4-D (51%) was obtained at the nanocatalyst amount of 2 g L^{-1}. The high ability of the advanced oxidation process in removal of toxins can be attributed to the production of hydroxyl radicals [38, 39].

Nanoparticles have much higher reactivity and much higher surface than common particles, which results in more hydroxyl radical production and subsequent degradation of insecticides [40]. In addition, active and available sites and the possibility of nanoparticles colliding with the pollutant increase by increasing the nanoparticles. On the other hand, increasing the amount of nanocatalysts results in more photon adsorption and hence more effect on the pollutant [41]. However, the cause of decrease in the efficiency of 2,4-D removal is related to excess amounts than the optimal dosage. The excessive doses may lead to the greater dispersion and increased turbidity by nanoparticles and consequently decreases in UV light penetration [42]. Therefore, 2 g L^{-1} of nanocomposite was selected as the optimal dose for the subsequent experiments.

Xu et al. [8] showed that the photocatalytic degradation efficiency of the 2,4-D increased by increasing the amount of nanocatalysts to 1.5 g L^{-1}. They also reported that more increase in nanocatalysis resulted in a decrease in the degradation efficiency. Moreover, the authors stated that more catalyst content would increase the availability of the entire surface and active sites [8]. On the other hand, the decrease in removal efficiency may occur due to the scattering of light and the decrease of light penetration in presence of excess catalyst [8]. Similar results were observed by Hosseini et al. [43] in a study on the removal of diazinone (53%) with 100 mg L^{-1} of cns-ZnO nanoparticles under a light diode lamp. In addition, Xiong and Hu [12] reported a removal efficiency over 90% for acetaminophen with a 0.01 g L^{-1} TiO_2 nanoparticles under the UVA/LED. Furthermore, Natarajan et al. [44] reported a 95% removal of Rhodamine B in a UV-LED/TiO_2 process using 1.6 g L^{-1} nanoparticles.

3.2.3 Effect of Initial Concentration 2,4-D

The initial concentration of pollutant is an important parameter affecting the photocatalytic degradation process. Figure 5c shows the effect of 2,4-D initial concentrations (10, 25, 50, 75, 100 mg L^{-1}) on the photocatalytic degradation efficiency using Mn doped ZnO/GO nanocomposite under a LED lamp. The results showed that the photocatalytic degradation efficiency decreased with an increase in the initial concentration of 2,4-D. The probable reason for this trend is that the increase of 2,4-D concentrations leads to

the adsorption of more 2,4-D on the nanocomposite surface due to the constant amount of nanoparticles. Therefore, the surface-active sites for adsorption of hydroxyl ions decrease. This leads the reduction of hydroxyl radicals (·OH) production, and thus degradation efficiency decrease [45]. Also, increasing the concentration of 2,4-D prevents reaching of photons to catalyst, resulting in a decrease in the photocatalytic degradation rate [1].

In several studies, the effect of initial concentrations of pollutants on the process efficiency have been studied and similar results have been reported. For instance, in a study on the photocatalytic degradation of diazinon under visible light, Mirmasoomi et al. [46] investigated the effect of diazinon concentration (from 10 to 30 mg L^{-1}) on the photocatalytic degradation using TiO_2/Fe_2O_3. Their results showed that under optimal conditions (catalytic dose of 0.1 g L^{-1}, light intensity of 14 W cm^{-2} at 45 min), the degradation efficiency was increased by about 90% with the decrease in the initial concentration of diazinon [46]. In another study on removal of 4-chlorophenol with advanced oxidation and microwave, Sidmohammadi et al. [47] obtained 81.7% removal at concentration of 50 mg L^{-1} after 90 min. On the other hand, they observed that the removal efficiency decreased to 16% after 90 min when the initial concentration increased to 500 mg L^{-1}.

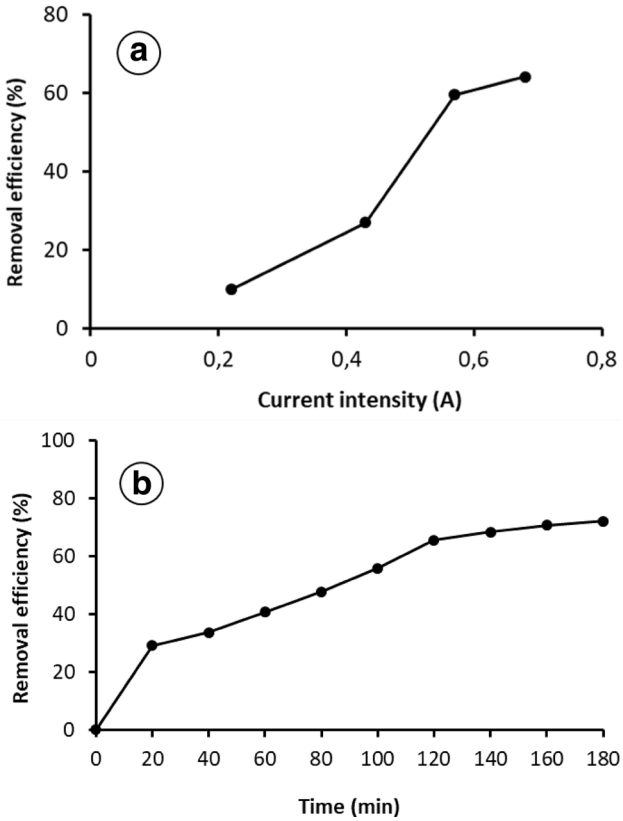

Fig. 6 **a** Influence of light intensity on the photocatalytic decomposition of 2,4-D using an LED lamp (pH 5; concentration of 2,4-D = 50 mg L^{-1} amount of Mn doped ZnO/GO = 2 g L^{-1}); and **b** Influence of run time on the photocatalytic decomposition of 2,4-D using an LED lamp (pH 5; constant concentration of 2,4-D = 50 mg/L; electrical current intensity = 0.68 A; amount of Mn doped ZnO/GO = 2 g L^{-1})

3.2.4 Effect of Light Intensity

The intensity of light emitted from a source is one of the most influential parameters in the photocatalytic processes. The effect of light intensity supplied from LED lamps (the intensity of light was measured at the reactor center by changing the electric current) in the photocatalytic decomposition of 2,4-D is depicted in Fig. 6a. The results of the study indicated that the 2,4-D removal efficiency also increased by increasing electrical current and the light intensity. The maximum removal efficiency of 64% was obtained at 0.68 A (1000 Lux). The number of stimulated electrons on the surface of the catalyst also increased by increasing the intensity of light, which resulted in production of more active hydroxyl radicals. The increased production and accumulation of active hydroxyl radicals (·OH) result in increased photocatalytic oxidation rate and elevated decomposition of environmental pollutants [48].

3.2.5 Effect of Run Time

The effect of run time (10–18 min) on the photocatalytic removal of 2,4-D under the light of an LED lamp is shown in Fig. 6b. As seen in Fig. 6b, the 2,4-D removal efficiency increased significantly by increasing the run time to 120 min, but the trend did not continue afterward and reached a balance. Therefore, the run time of 120 min was considered as the optimum time. The most likely explanation is the increased opportunity of the photocatalytic particles to participate in the photocatalytic reactions. The formation of photogenerated oxidative valence holes (h^+) on the surface of the nanoparticles increases over time, and accordingly, the active sites on the surface of the catalyst become easily accessible. These sites become occupied by increasing the concentration of the pollutants, and consequently, the removal efficiency reduces [49, 50]. Many studies have been conducted in this field, and all reported the reduced removal efficiency of different pollutants over time. In a study conducted by Mousavi et al. [51], it was reported that the diazinon removal efficiency was 33.8%, 69.9%, and 78.6%, respectively, under 0.1, 0.2, and 0.3 g L^{-1} of NH_4Cl^--stimulated active carbon in the first 2 min of the reaction. Moreover, it was observed that the removal efficiency increased to 63.6%, 89.7%, and 96.7%, respectively, until the run time of 30 min.

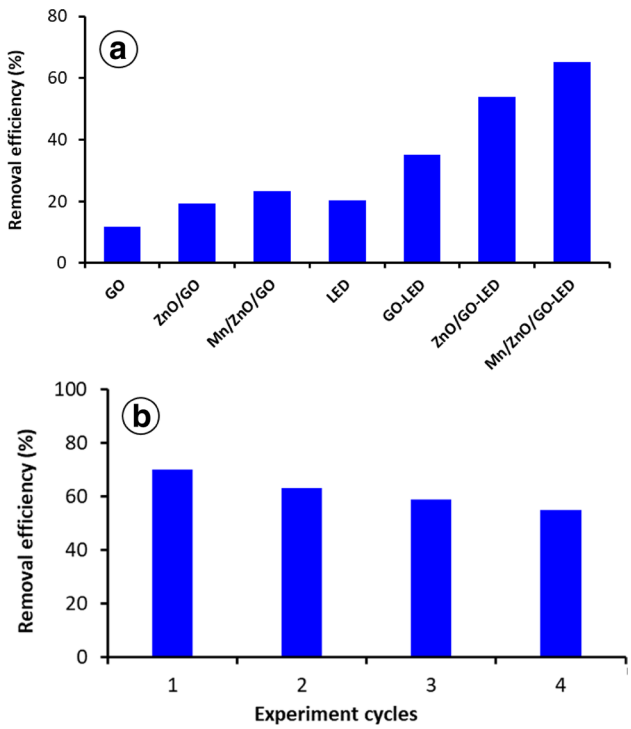

Fig. 7 **a** Comparison of the photocatalytic decomposition processes of 2,4-D (pH 5; initial concentration of the poison = 10 mg L^{-1}; electrical current intensity = 0.68 A; amount of nanocomposite Mn doped ZnO/GO = 2 g L^{-1}); and **b** Reusability of Mn doped ZnO/GO nanocomposite in the photocatalytic decomposition of 2,4-D (pH 5; initial concentration of the poison = 10 mg L^{-1} electrical current intensity = 0.68 A; amount of nanocomposite Mn doped ZnO/GO = 2 g L^{-1})

3.2.6 Effect of Photocatalytic Process Efficiency

Figure 7a shows the synergistic effect of 2,4-D on the photocatalytic removal efficiency at optimum conditions. As illustrated in Fig. 7a, the 2,4-D removal efficiency for GO, GO-ZnO, Mn doped ZnO/GO, LED, GO/LED, GO-ZnO/LED, and Mn doped ZnO/GO/LED was 12%, 19%, 23%, 20%, 35%, 53%, and 67%, respectively. As shown in Fig. 7a, the 2,4-D removal efficiency for LED and Mn doped ZnO/GO was low separately, whereas it was high for the integrated Mn doped ZnO/GO/LED.

For the photocatalytic decomposition of organic compounds, semi-conductive optical stimulation followed by the formation of electron–hole pairs is used at the surface of the catalyst. A high oxidative potential of the hole (h^{+}_{VB}) in the catalyst facilitates the direct oxidation of organic compounds (insecticide). Also, the breakdown of water or reaction of the hole with hydroxyl radicals (·OH) results in the formation of highly reactive radicals. These radicals are strong non-selective oxidative agents which accelerate the degradation of organic compounds. The electron in the conduction band of the catalyst surface converts the oxygen molecules into anion peroxides. Such radicals create organic peroxides or hydrogen peroxide in the presence of organic compounds. In addition, the electrons in the conduction band are responsible for the fabrication of ·OH which is the main agent in the mineralization of organic compounds [52, 53].

3.2.7 Reusability of the Synthesized Nanocomposite

One of the important factors in evaluating the use of adsorbents and catalysts is their reusability [54]. In this study, the reusability of the nanocomposite was investigated by four successive photocatalysis experiment cycles. At the end of each cycle, the nanocomposite catalysts were separated by centrifugation and were washed several times by distilled water. After they had been acid-washed, their reusability was determined through four cycles. The 2,4-D removal efficiency of the Mn-doped ZnO/GO nanocomposite is shown in Fig. 7b. As seen from this figure, the removal efficiency of nanocomposite decreased by about 13% (from 70 to 57%), indicating that the studied catalyst retained its ability to remove 2,4-D. The slight decrease that was occurred at each stage might be due to the fact that the decomposition products remained on the catalyst surfaces during photocatalytic reactions and reduced its photocatalytic activity [55].

4 Conclusions

Nanophotocatalyst characteristics (SEM, AFM, DLS, Zeta potential, XRD, and FTIR) indicated that the synthesis of Mn-doped ZnO/GO nanocomposite could be conducted successfully under LED radiation. The photocatalytic degradation efficiency was increased by increasing the amount of Mn-doped ZnO/GO nanocatalyst from 0.5 to 3 g L^{-1} and pH from 3 to 5. On the other hand, increasing the initial concentration of 2,4-D caused a decrease in the photocatalytic degradation efficiency. About 67% of 2,4-D removal could be achieved by using Mn-doped ZnO/GO nanocomposite at an initial pH of 5, 25 mg L^{-1} of 2,4-D, 2 g L^{-1} of nanocomposite, 10 mg L^{-1} of zinc, and 120 min of contact time. Based on the experimental findings obtained within the framework of the present study, it was concluded that the synthesis of Mn-doped ZnO/graphene nanocomposite under LED radiation could be an efficient method for the photocatalytic degradation of 2,4-D under LED radiation.

Acknowledgements The authors offer their special thanks to the sponsors of the project.

Funding This manuscript is extracted from the project approved by the Environmental Health Research Center and funded by the Kurdistan University of Medical Sciences (Grant No. IR.MUK.REC.1395/236).

Compliance with Ethical Standards

Conflict of interest The authors declare that there are no conflicts of interest including any financial, personal, or other relationships with other people or organizations.

Research Involving Human and Animal Participants This article does not contain any studies with human participants or animals performed by any of the authors.

References

1. K. Del Ãngel-Sanchez, O. Vaquez-Cuchillo, A. Aguilar-Elguezabal, A. Cruz-Lopez, A. Herrera-Gomez, Photocatalytic degradation of 2,4-dichlorophenoxyacetic acid under visible light: effect of synthesis route. Mater. Chem. Phys. **139**, 423–430 (2013)
2. P. Qiu, J. Yao, H. Chen, F. Jiang, X. Xie, Enhanced visible-light photocatalytic decomposition of 2,4-dichlorophenoxyacetic acid over $ZnIn_2S_4$/g-C_3N_4 photocatalyst. J. Hazard. Mater. **317**, 158–168 (2016)
3. Y. Tang, S. Luo, Y. Teng, C. Liu, X. Xu, X. Zhang, L. Chen, Efficient removal of herbicide 2,4-dichlorophenoxyacetic acid from water using Ag/reduced graphene oxide co-decorated TiO2 nanotube arrays. J. Hazard. Mater. **241**, 323–330 (2012)
4. A. Nasser, U. Mingelgrin, Birnessite-induced mechanochemical degradation of 2,4-dichlorophenol. Chemosphere **107**, 175–179 (2014)
5. H.B. Senturk, D. Ozdes, A. Gundogdu, C. Duran, M. Soylak, Removal of phenol from aqueous solutions by adsorption onto organomodified Tirebolu bentonite: equilibrium, kinetic and thermodynamic study. J. Hazard. Mater. **172**, 353–362 (2009)
6. M. Raoov, S. Mohamad, M.R. Abas, Removal of 2,4-dichlorophenol using cyclodextrin-ionic liquid polymer as a macroporous material: characterization, adsorption isotherm, kinetic study, thermodynamics. J. Hazard. Mater. **263**, 501–516 (2013)
7. Y. Li, X. Li, Y. Li, J. Qi, J. Bian, Y. Yuan, Selective removal of 2,4-dichlorophenol from contaminated water using non-covalent imprinted microspheres. Environ. Pollut. **157**, 1879–1885 (2009)
8. R. Xu, Q. Zhou, F. Li, B. Zhang, Laccase immobilization on chitosan/poly (vinyl alcohol) composite nanofibrous membranes for 2,4-dichlorophenol removal. Chem. Eng. J. **222**, 321–329 (2013)
9. M. Caetano, C.S. Valderrama, A. Farran, J.L. Cortina, Phenol removal from aqueous solution by adsorption and ion exchange mechanisms onto polymeric resins. J. Colloid Interface Sci. **338**, 402–409 (2009)
10. M.-R. Samarghandi, J.-K. Yang, O. Giahi, M. Shirzad-Siboni, Photocatalytic reduction of hexavalent chromium with illuminated amorphous FeOOH. Environ. Technol. **36**, 1132–1140 (2015)
11. Z. Wang, J. Liu, Y. Dai, W. Dong, S. Zhang, J. Chen, CFD modeling of a UV-LED photocatalytic odor abatement process in a continuous reactor. J. Hazard. Mater. **215**, 25–31 (2012)
12. P. Xiong, J. Hu, Degradation of acetaminophen by UVA/LED/TiO_2 process. Sep. Purif. Technol. **91**, 89–95 (2012)
13. B. Shahmoradi, A. Maleki, K. Byrappa, Removal of disperse orange 25 using in situ surface-modified iron-doped TiO_2 nanoparticles. Desalin. Water Treat. **53**, 3615–3622 (2015)
14. B. Shahmoradi, M. Negahdary, A. Maleki, Hydrothermal synthesis of surface-modified, manganese-doped TiO_2 nanoparticles for photodegradation of methylene blue. Environ. Eng. Sci. **29**, 1032–1037 (2012)
15. A. Maleki, M. Safari, R. Rezaee, R.D. Cheshmeh Soltani, B. Shahmoradi, Y. Zandsalimi, Photocatalytic degradation of humic substances in the presence of ZnO nanoparticles immobilized on glass plates under ultraviolet irradiation. Sep. Sci. Technol. **51**, 2484–2489 (2016)
16. R. DarvishiCheshmehSoltani, A. Khataee, M. Mashayekhi, M. Safari, Photocatalysis of formaldehyde in the aqueous phase over ZnO/diatomite nanocomposite. Turk. J. Chem. **40**, 402–411 (2016)
17. A. Maleki, M. Safari, B. Shahmoradi, Y. Zandsalimi, H. Daraei, F. Gharibi, Photocatalytic degradation of humic substances in aqueous solution using Cu-doped ZnO nanoparticles under natural sunlight irradiation. Environ. Sci. Pollut. Res. **22**, 16875–16880 (2015)
18. Y.H. Siddique, W. Khan, S. Khanam, S. Jyoti, F. Naz, B.R. Singh, A.H. Naqvi, Toxic potential of synthesized graphene zinc oxide nanocomposite in the third instar larvae of transgenic *Drosophila melanogaster* (*hsp70-lacZ*) Bg^9. Biomed. Res. Int. **2014**, 1–10 (2014)
19. M. Ahmad, E. Ahmed, W. Ahmed, A. Elhissi, Z.L. Hong, N.R. Khalid, Enhancing visible light responsive photocatalytic activity by decorating Mn-doped ZnO nanoparticles on graphene. Ceram. Int. **40**, 10085–10097 (2014)
20. M. Salari, F. Changani, M. DarvishMotevali, S. Akbari, Evaluation of the removal of 2ØŒ 4 dichlorophenol by chitosan from aqueous solutions. J. Environ. Health Eng. **2**, 198–210 (2015)
21. B.N. Dole, V.D. Mote, V.R. Huse, Y. Purushotham, M.K. Lande, K.M. Jadhav, S.S. Shah, Structural studies of Mn doped ZnO nanoparticles. Curr. Appl. Phys. **11**, 762–766 (2011)
22. R. Ullah, J. Dutta, Photocatalytic degradation of organic dyes with manganese-doped ZnO nanoparticles. J. Hazard. Mater. **156**, 194–200 (2008)
23. S. Ishaq, M. Moussa, F. Kanwal, M. Ehsan, M. Saleem, T.N. Van, D. Losic, Facile synthesis of ternary graphene nanocomposites with doped metal oxide and conductive polymers as electrode materials for high performance supercapacitors. Sci. Rep. **9**, 5974 (2019)
24. A.A. Elzatahry, A.M. Abdullah, T.A.S. El-Din, A.M. Al-Enizi, A.A. Maarouf, A. Galal, H.K. Hassan, E.H. El-Ads, S.S. Al-Theyab, A.A. Al-Ghamdi, Nanocomposite graphene-based material for fuel cell applications. Int. J. Electrochem. Sci. **7**, 3115–3126 (2012)
25. F.T. Johra, J.W. Lee, W.G. Jung, Facile and safe graphene preparation on solution based platform. J. Ind. Eng. Chem. **20**, 2883–2887 (2014)
26. N.I. Zaaba, K.L. Foo, U. Hashim, S.J. Tan, W.W. Liu, C.H. Voon, Synthesis of graphene oxide using modified hummers method: solvent influence. Proced. Eng. **184**, 469–477 (2017)
27. J. Liu, H. Bai, Y. Wang, Z. Liu, X. Zhang, D.D. Sun, Self-assembling TiO2 nanorods on large graphene oxide sheets at a two-phase interface and their anti-recombination in photocatalytic applications. Adv. Func. Mater. **20**, 4175–4181 (2010)
28. M. Nithya, Electrochemical sensing of ascorbic acid on ZnO-decorated reduced graphene oxide electrode. J. Biosens. Bioelectron. **6**, 1–9 (2015)
29. P.K. Labhane, L.B. Patle, G.H. Sonawane, S.H. Sonawane, Fabrication of ternary Mn doped ZnO nanoparticles grafted on reduced graphene oxide (RGO) sheet as an efficient solar light driven photocatalyst. Chem. Phys. Lett. **710**, 70–77 (2018)
30. S. Sarkar, D. Basak, The reduction of graphene oxide by zinc powder to produce a zinc oxide-reduced graphene oxide hybrid and its superior photocatalytic activity. Chem. Phys. Lett. **561**, 125–130 (2013)
31. O.D. Jayakumar, I.K. Gopalakrishnan, R.M. Kadam, A. Vinu, A. Asthana, A.K. Tyagi, Magnetization and structural studies

of Mn doped ZnO nanoparticles: prepared by reverse micelle method. J. Cryst. Growth **300**, 358–363 (2007)
32. S. Kashyap, S. Mishra, S.K. Behera, Aqueous colloidal stability of graphene oxide and chemically converted graphene. J. Nanopart. **2014**, 1–6 (2014)
33. H.S. Shin, D. Kang, Control of size and physical properties of graphene oxide by changing the oxidation temperature. Carbon Lett. **13**, 39–43 (2012)
34. P.R. Gogate, A.B. Pandit, A review of imperative technologies for wastewater treatment I: oxidation technologies at ambient conditions. Adv. Environ. Res. **8**, 501–551 (2004)
35. S. Hyun, L.S. Lee, Quantifying the contribution of different sorption mechanisms for 2,4-dichlorophenoxyacetic acid sorption by several variable-charge soils. Environ. Sci. Technol. **39**, 2522–2528 (2005)
36. A. Azari, M. Salari, M.H. Dehghani, M. Alimohammadi, H. Ghaffari, K. Sharafi, N. Shariatifar, M. Baziar, Efficiency of magnitized graphene oxide nanoparticles in removal of 2,4-dichlorophenol from aqueous solution. J. Mazandaran Univ. Med. Sci. **26**, 265–281 (2017)
37. R. Piri, M. Kermani, A. Esrafili, Using persulfate-based photochemical oxidation (UV/NA2s2o8) in eliminating 4-chlorophenol from aqueous solutions. J. Mazandaran Univ. Med. Sci. **27**, 358–370 (2017)
38. A. Maleki, Y. Zandsalimi, B. Shahmoradi, R. Rezaie, M.A. Pordel, Comparison of the efficiency of photochemical processes combined with UV/H_2O_2 and UV/TiO_2 in removal of Acid Red 18 from aqueous solutions. Sci. J. Kurd. Univ. Med. Sci. **16**, 101–108 (2011)
39. A. Maleki, B. Shahmoradi, Solar degradation of Direct Blue 71 using surface modified iron doped ZnO hybrid nanomaterials. Water Sci. Technol. **65**, 1923–1928 (2012)
40. F. He, D. Zhao, J. Liu, C.B. Roberts, Stabilization of Fe-Pd nanoparticles with sodium carboxymethyl cellulose for enhanced transport and dechlorination of trichloroethylene in soil and groundwater. Ind. Eng. Chem. Res. **46**, 29–34 (2007)
41. R. Darvishi Cheshmeh Soltani, A. Rezaee, M. Safari, A.R. Khataee, B. Karimi, Photocatalytic degradation of formaldehyde in aqueous solution using ZnO nanoparticles immobilized on glass plates. Desalin. Water Treat. **53**, 1613–1620 (2015)
42. N. Kashif, F. Ouyang, Parameters effect on heterogeneous photocatalysed degradation of phenol in aqueous dispersion of TiO_2. J. Environ. Sci. **21**, 527–533 (2009)
43. H. Hossaini, G. Moussavi, M. Farrokhi, Oxidation of diazinon in cns-ZnO/LED photocatalytic process: catalyst preparation, photocatalytic examination, and toxicity bioassay of oxidation by-products. Sep. Purif. Technol. **174**, 320–330 (2017)
44. T.S. Natarajan, M. Thomas, K. Natarajan, H.C. Bajaj, R.J. Tayade, Study on UV-LED/TiO2 process for degradation of Rhodamine B dye. Chem. Eng. J. **169**, 126–134 (2011)
45. D. Mijin, M. Savic, P. Snezana, A. Smiljanic, O. Glavaski, M. Jovanovic, S. Petrovic, A study of the photocatalytic degradation of metamitron in ZnO water suspensions. Desalination **249**, 286–292 (2009)
46. S.R. Mirmasoomi, M. Mehdipour Ghazi, M. Galedari, Photocatalytic degradation of diazinon under visible light using TiO_2/Fe_2O_3 nanocomposite synthesized by ultrasonic-assisted impregnation method. Sep. Purif. Technol. **175**, 418–427 (2017)
47. A. Sidmohammadi, G. Asgari, A. Ebrahimi, Z. Sharifi, A.H. Movahedian, 4-Chlorophenol oxidation combined with the application of advanced oxidation technology and the modified microwave in chemical and petrochemical wastewater industry. Health Syst. Res. **6**, 390–396 (2010)
48. S. Akhtar, A.A. Khan, Q. Husain, Potential of immobilized bitter gourd (Momordica charantia) peroxidases in the decolorization and removal of textile dyes from polluted wastewater and dyeing effluent. Chemosphere **60**, 291–301 (2005)
49. H. Chen, H. Luo, Y. Lan, T. Dong, B. Hu, Y. Wang, Removal of tetracycline from aqueous solutions using polyvinylpyrrolidone (PVP-K30) modified nanoscale zero valent iron. J. Hazard. Mater. **192**, 44–53 (2011)
50. D. Shao, X. Wang, Q. Fan, Photocatalytic reduction of Cr(VI) to Cr(III) in solution containing ZnO or ZSM-5 zeolite using oxalate as model organic compound in environment. Microporous Mesoporous Mater. **117**, 243–248 (2009)
51. G. Moussavi, H. Hosseini, A. Alahabadi, The investigation of diazinon pesticide removal from contaminated water by adsorption onto NH_4Cl-induced activated carbon. Chem. Eng. J. **214**, 172–179 (2013)
52. A.A. Khodja, T. Sehili, J.-F.O. Pilichowski, P. Boule, Photocatalytic degradation of 2-phenylphenol on TiO_2 and ZnO in aqueous suspensions. J. Photochem. Photobiol., A **141**, 231–239 (2001)
53. I.K. Konstantinou, T.A. Albanis, TiO_2-assisted photocatalytic degradation of azo dyes in aqueous solution: kinetic and mechanistic investigations: a review. Appl. Catal. B **49**, 1–14 (2004)
54. K. Vignesh, M. Rajarajan, A. Suganthi, Visible light assisted photocatalytic performance of Ni and Th co-doped ZnO nanoparticles for the degradation of methylene blue dye. J. Ind. Eng. Chem. **20**, 3826–3833 (2014)
55. E. Topkaya, M. Konyar, H.C. Yatmaz, K. Öztürk, Pure ZnO and composite ZnO/TiO_2 catalyst plates: a comparative study for the degradation of azo dye, pesticide and antibiotic in aqueous solutions. J. Colloid Interface Sci. **430**, 6–11 (2014)